Regular paper

Effect of ultrasonic cavitation on measurement of sound pressure using hydrophone

Tam Thanh Nguyen[1,2*], Yoshiyuki Asakura[3], Nagaya Okada[3], Shinobu Koda[4], and Keiji Yasuda[1*]

[1]*Department of Chemical Engineering, Graduate School of Engineering, Nagoya University, Nagoya 464-8603, Japan*

[2]*Faculty of Environment, University of Science, VNU-HCM, Vietnam*

[3]*Honda Electronics Co., Ltd., Toyohashi, Aichi 441-3193, Japan*

[4]*Department of Molecular Design and Engineering, Graduate School of Engineering, Nagoya University, Nagoya 464-8603, Japan*

E-mail: nguyen.thanh.tam@e.mbox.nagoya-u.ac.jp; yasuda@nuce.nagoya-u.ac.jp

Effect of ultrasonic cavitation on sound pressure at the fundamental, second harmonic, and first ultraharmonic frequencies was investigated from low to high ultrasonic intensities. The driving frequencies were 22, 304, and 488 kHz. Sound pressure was measured using a needle-type hydrophone and ultrasonic cavitation was estimated from the broadband integrated pressure (BIP). With increasing square root of electric power applied to a transducer, the sound pressure at the fundamental frequency linearly increased initially, dropped at approximately the electric power of cavitation inception, and afterward increased again. The sound pressure at the second harmonic frequency was detected just below the electric power of cavitation inception. The first ultraharmonic component appeared at around the electric power of cavitation inception at 304 and 488 kHz. However, at 22 kHz, the first ultraharmonic component appeared at a higher electric power than that of cavitation inception.

1. Introduction

High-intensity ultrasound in liquid has practical applications such as ultrasonic cleaning, homogenization,[1] and atomization,[2,3] and has potential applications in extraction,[4] emulsification,[5] crystallization,[6] sonochemical reactions,[7-9] droplet coalescence,[10] pharmaceutical processing,[11] and therapy.[12-15] The evaluation of sound intensity in liquid is important for the development of ultrasonic devices. Sound intensity was evaluated by, for example, sound pressure measurement,[16] radiation force measurement,[17] and calorimetry.[18]

Among these techniques, sound pressure measurement has been proposed as a particularly effective method to obtain the spatial distribution of sound pressure.[19] For example, the measurement of sound pressure distribution in a cleaner is important to analyze the nonuniform sound field when continuous ultrasound is irradiated and a standing wave is formed.[20] In sound pressure measurement, a hydrophone is normally used. As the sound intensity in liquid increases, small bubbles occur, grow, and collapse. The collapse of bubbles induces high temperature, high pressure, and high liquid velocity near the bubbles. This phenomenon is called ultrasonic cavitation. Since a hydrophone easily breaks owing to ultrasonic cavitation, the sound pressure measurement using a continuous wave at a high sound intensity has not been sufficiently conducted in a wide range of driving ultrasonic frequencies. Recently, our group has developed a tough needle-type hydrophone fabricated by a hydrothermal synthesis method. This hydrophone can measure high sound pressures in a wide range of ultrasonic frequencies within which a high-intensity continuous ultrasound is irradiated and many cavitation bubbles occur.[21-22]

Theoretically, sound intensity is proportional to the effective electric input power applied to a transducer.[23] Thus, sound pressure is proportional to square root of electric input power. However, Neppiras reported that the sound pressure received from a microphone decreased rapidly in the vicinity of the applied sound pressure of cavitation inception.[16] He detected the cavitation inception from the appearance of broadband noise. He also measured the subharmonic (fundamental frequency divided by integer) component and reported that the subharmonic signal drastically arose in the vicinity of the applied sound pressure of cavitation inception, and visible bubbles were observed. Broadband noise has been utilized by several researchers to detect cavitation generation.[24-26] Additionally, the harmonic frequency (integer multiples of fundamental frequency) component has been used as an indicator of bubble generation.[27] The

effect of driving frequency on the relationship between the broadband noise and the sound pressures of the fundamental, harmonic, and subharmonic frequencies was little investigated.

For the evaluation of an ultrasonic apparatus, it is important to measure the sound pressures of some components in the presence of cavitation bubbles. In this study, a broadband integrated pressure (BIP) was used to estimate the broadband noise. The BIP and sound pressures at the fundamental (f_1), second harmonic (f_2), and first ultraharmonic (1.5 multiples of fundamental, $f_{1.5}$) frequencies were measured using a tough needle-type hydrophone with increasing effective input power applied to a transducer. The driving frequencies of the transducer were 22, 304, and 488 kHz. To visualize bubbles in the presence of cavitation, ultrasonic diagnostic equipment was used.

2. Experimental methods

2.1 Apparatus

The experimental apparatus for the measurement of sound pressure and broadband noise is shown in Fig. 1. The vessel was made from stainless steel. The inner diameter of the vessel was 56.8 mm. A Langevin transducer and disc transducers were selectively used at low and high driving frequencies, respectively. A Langevin transducer 45 mm in diameter at 22 kHz, and disc transducers 50 mm in diameter at 304 and 488 kHz were used. The transducer was fixed at the bottom of the vessel, and ultrasound was irradiated onto the water in the vessel. A fan was attached to cool the transducer. A water bath was used to control the sample temperature at 298 K.

To measure sound pressure in a wide range of frequencies, the tough needle-type hydrophone (Honda Electronics HUS-200S) was submerged into water at the position of highest sound pressure. The hydrophone position was precisely adjusted by an XYZ-axis stage and a stage controller (Sigmakoki SHOT-204). The hydrophone was connected to a spectrum analyzer (HP 8595E) through a preamplifier (Honda Electronics HUS-200A). The preamplifier was used to convert impedance. The electric power applied to the transducer was calculated from the voltage of both ends of the transducer measured using an oscilloscope (Tektronix TDS3014B) and current through the transducer measured using a current probe (Tektronix TCP202). The effective electric power was transferred to a personal computer via a general-purpose interface bus (GPIB). A continuous sinusoidal wave signal was generated by a signal generator (NF

WF1974) and amplified by a power amplifier (E&I 1040L). The output waveform amplitude of the signal generator was set by the personal computer via GPIB. At 22 kHz, an impedance matching circuit was connected between the amplifier and the transducer. To keep the electric power applied to the transducer constant, the amplitude of the signal was controlled using a program (Honda Electronics) and the personal computer.

It is reported that a hysteresis effect was observed in sound pressures at harmonic and subharmonic frequencies, and broadband noise when the sound intensity changed.[27] In order to inhibit the hysteresis effect, sound pressure measurement was carried out by increasing the electric power applied to the transducer. The sample was air-saturated distilled water. The sample volume was 100 mL. Before the measurement was performed, the resonance condition of the water in the vessel was set by adjusting driving frequency.

2.2. BIP and sound pressures at fundamental, harmonic, and ultraharmonic frequencies

In this study, BIP was utilized as the broadband noise to estimate the ultrasonic cavitation generated in water. Figure 2 shows an example of a sound pressure spectrum at a driving frequency of 304 kHz measured using the tough needle-type hydrophone when the effective electric input power applied to the transducer is 4 W. This hydrophone was calibrated sound pressure in the frequency range from 20 kHz to 20 MHz. BIP was calculated using the following equation:

$$\mathrm{BIP} = \int_{f_s}^{f_e} [P_S(f) - P_N(f)]\, df\,, \qquad (1)$$

where $P_S(f)$ represents the broadband sound pressures excluding the fundamental, harmonic, subharmonic, and ultraharmonic components, and $P_N(f)$ represents the sound pressures of the background noise. The start frequency of the integration region f_s was decided as 20 kHz and the end frequency f_e was 20 MHz for all driving frequencies. The BIP is the shaded area in Fig. 2. It is noted that the unit of sound pressure is dB.

Acoustic signals at the fundamental, second harmonic and first ultraharmonic frequencies were obtained using the tough needle-type hydrophone, preamplifier, and spectrum analyzer. The signals were converted to sound pressure.

3. Results and discussion

3.1. Sound pressure at fundamental frequency and BIP at low electric power

Figure 3 shows the sound pressure at the fundamental frequency and the BIP as functions of the square root of the effective electric power applied to the transducer. The broadband noise has been used as an indicator of ultrasonic cavitation. The broadband noise is generated by the temporal fluctuation in the number of bubbles owing to the fragmentation of cavitation bubbles of various sizes. The shockwaves emitted from cavitation bubbles are also detected by a hydrophone as vibrations, which provides the broadband noise component.[28,29] In Fig. 3(a), the driving frequency is 22 kHz and the electric power changes from 0 to 9 W. As the square root of the electric power increases, the sound pressure at the fundamental frequency becomes proportional to the square root of electric input power. This linear increment agrees with theory.[23] The electric power at which the BIP starts to appear is defined as the electric power of cavitation inception. In the vicinity of the square root of the electric power of cavitation inception, the sound pressure at the fundamental frequency, however, instantaneously decreases. A similar trend of unstable changes in sound pressure was reported by Neppiras.[16] The sound pressure decreased notably around cavitation inception. Attenuation by cavitation bubbles explained the decrease in sound pressure at the fundamental frequency. The BIP increases with electric power above the electric power of cavitation inception.

In the case of 304 kHz, a similar trend of changes in sound pressure at the fundamental frequency and the BIP as 22 kHz is observed. In Fig. 3(b), the driving frequency is 488 kHz. The sound pressure at the fundamental frequency drops drastically in the vicinity of the electric power of cavitation inception and becomes almost zero. It is considered that numerous cavitation bubbles were generated in water.

To clarify the existence of bubbles in water under ultrasonic irradiation, ultrasonic diagnostic equipment (Honda Electronics HS–2100) with a 10 MHz probe (Honda Electronics HLS–513M) was used. This equipment enables the visualization of fine bubbles with several ten micrometers in diameter. Figure 4(a) shows an experimental setting for the bubble observation. The ultrasound irradiation system was the same as that for the measurement of sound pressure. Ultrasound was irradiated horizontally by an immersed transducer. The probe was located between the hydrophone and the transducer. To reflect ultrasound at the same proportion at the

water surface, a polystyrene foam reflector was used.

Figures 4(b) and 4(c) show images of the ultrasonic diagnostic equipment in water when the driving frequency is 488 kHz and the effective electric power applied to the transducer is 1 W. In the absence of ultrasonic irradiation, the image in Fig. 4(b) is black as a whole, which implies that no bubbles exist in water. On the other hand, in the presence of ultrasound irradiation, many white dots indicating bubbles in water are observed in Fig. 4(c), and the horizontal interval of dots corresponds to one half of ultrasonic wavelength in water. This result indicates the presence of many bubbles trapped in standing waves of ultrasound. Since the ultrasound at a high frequency has a short wavelength, the number density of bubbles is high in water. Bubbles might be attached onto the hydrophone surface. These bubbles largely obstruct the detection of sound pressure. This is the reason why the sound pressure at a fundamental frequency of 488 kHz drastically dropped above the electric power of cavitation inception.

3.2. Sound pressure at fundamental frequency and BIP at high electric power

Figure 5 shows the sound pressure at the fundamental frequency and the BIP as functions of the square root of the effective electric power applied to the transducer when the electric power changes from 0 to 100 W. In Fig. 5(a), the driving frequency is 22 kHz. As square root of electric power increases, the sound pressure at the fundamental frequency linearly increases initially, decreases around cavitation inception and then increases again. However at a very high electric power, the sound pressure no longer increases and becomes unstable. The BIP rises above the square root of the electric power of cavitation inception and also does not increase at a very high electric power.

The effective measurement range of this hydrophone was investigated in degassed water. The sound pressure at the fundamental frequency increased linearly with increasing square root of the electric power applied to the transducer until the sound pressure reached approximately 8 MPa.[30] From this result, it is clear that the sound pressure in Fig. 5(a) is within the effective measurement range. To check the conversion efficiency of the transducer from electric power to ultrasonic power above the electric power of cavitation inception, the ultrasonic power in water was measured by calorimetry.[18] The ultrasonic power was proportional to the effective electric power applied to the transducer at high electric powers. This result means that the electric power applied to the transducer is properly converted into ultrasonic power under these

experimental conditions.

Cavitation bubbles at low driving frequencies are larger than those at high driving frequencies.[31-33] The instability of sound pressure at a high electric power might be explained by the existence of large bubbles in water and on the hydrophone surface. Consequently, the existence of those large bubbles enhances scattering and absorbance of ultrasound in water.

In Fig. 5(b), the driving frequency is 488 kHz. Both the sound pressure at the fundamental frequency and BIP increase with electric power above the cavitation inception. At a high electric power, the sound pressure in the reflected wave is significantly lower than that in the incident wave owing to ultrasonic attenuation by a great amount of cavitation bubbles and water and this enhances an acoustic radiation force. The ultrasonic attenuation is enhanced with increasing driving frequency. From these facts, trapped bubbles on the hydrophone surface and in standing waves are mostly removed by the acoustic radiation force. Therefore, the sound pressure increases again at a high electric power.

However, at a high electric power, in Figs. 5(a) and 5(b), the sound pressures are lower than the values extrapolated from the linear relationship between the sound pressure at the fundamental frequency and the square root of the electric power below the square root of the electric power of cavitation inception. This can be explained by the absorption and scattering caused by bubbles in water.

3.3. Sound pressure at the second harmonic and first ultraharmonic frequencies

Figure 6 shows the sound pressures at the second harmonic (f_2) and first ultraharmonic ($f_{1.5}$) frequencies as functions of the square root of the effective electric power applied to the transducer. In Fig. 6(a), at 22 kHz, as the square root of the electric power increases, the sound pressure at the second harmonic frequency is zero initially and increases. The square root of the electric power of inception of the second harmonic frequency is slightly lower than that of cavitation inception. Harmonic signals are derived from nonlinear oscillations of stable bubbles in water.[16] When the driving frequency is above 1 MHz, the nonlinear propagation of ultrasound affects the harmonic signals.[29] In this study, the effect of nonlinear propagation of ultrasound is small. As the electric power applied to the transducer increases, bubbles occur at first, then oscillate with ultrasound, and collapse at a high electric power, that is, ultrasonic cavitation is generated. This explains why the second harmonic component of sound pressure appears below

the electric power of cavitation inception.

The generation of half-order subharmonics is mainly attributed to the sound waves from relatively large bubbles, which oscillate with a doubled period of driving frequency.[29] From a Fourier series, the spectrum of any arbitrary periodic function with doubled period of driving frequency consists of the half-order subharmonics and ultraharmonics (integer multiples of subharmonics excluding the fundamental and harmonics) such as the first ultraharmonic, $f_{1.5}$. At first, the sound pressure at the first ultraharmonic frequency is zero, and then with increasing electric power, it increases at a relatively high electric power. The square root of the electric power of inception of the first ultraharmonic is higher than that of cavitation inception. From this result, it is thought that there are few relatively large bubbles oscillating with a doubled period in the vicinity of the electric power of cavitation inception, and large bubbles are formed by coalescence of bubbles at a high electric power.

When the driving frequencies are 304 and 488 kHz, as shown in Figs. 6(b) and 6(c), respectively, the electric power of inception of the second harmonic is lower than that of cavitation inception. The same behavior is observed at 22 kHz, as shown in Fig. 6(a). However, the square root of the electric power of cavitation inception of the first ultraharmonic at 304 kHz is slightly higher than that of cavitation inception, and the square root of the electric power of inception of the first ultraharmonic at 488 kHz is almost the same as that of cavitation inception. From these results, at a higher driving frequency, it is considered that large bubbles easily form at the electric power of cavitation inception. At 488 kHz, the sound pressures at the second harmonic and first ultraharmonic frequencies are small where the square root of electric power is from 0.5 to 1.5 $W^{0.5}$. This is because the number density of bubbles is high and many cavitation bubbles are trapped at the standing waves, as shown in Fig. 3(b).

4. Conclusions

In this study, we investigated how the ultrasonic cavitation affects the sound pressures at the fundamental, second harmonic, and first ultraharmonic frequencies, and BIP using the tough needle-type hydrophone. For the fundamental frequency, sound pressure increased linearly with increasing square root of the effective electric power when there were no cavitation bubbles in water. On the other hand, sound pressure drastically decreased at around the electric power of cavitation inception because of ultrasonic attenuation, caused by numerous bubbles trapped in

standing waves and on the hydrophone surface. Above the electric power of cavitation inception, sound pressure increased again. The possible reason is that trapped bubbles were mostly removed by the acoustic radiation force. However, at a high electric power, the sound pressure was lower than the value extrapolated from the linear relationship between the sound pressure at the fundamental frequency and the square root of electric power below the electric power of cavitation inception.

For the second harmonic signal, the electric power of inception was relatively lower than that of cavitation inception. This means that stable bubbles are generated at a lower electric power than cavitation bubbles. The first ultraharmonic component was detected near the electric power of cavitation inception at 304 and 488 kHz, and above that at 22 kHz. It is considered that at low driving frequencies, relatively large bubbles that oscillate with a doubled period were few at the electric power of cavitation inception and large bubbles were formed by coalescence of bubbles at a high electric power.

References

1) F. Martinez, A. Davidson, J. Anderson, S. Nakai, I. Desai, and A. Radcliffe, Nutr. Res. **12**, 561 (1992).
2) K. Yasuda, H. Honma, Z. Xu, Y. Asakura, and S. Koda, Jpn. J. Appl. Phys. **50**, 07HE23 (2011).
3) A. Endo, M. Yanagimoto, T. Asami, and H. Miura, Jpn. J. Appl. Phys. **54**, 07HE13 (2015).
4) M. Vinatoru, Ultrason. Sonochem. **8**, 303 (2001).
5) G. Cravotto, L. Boffa, S. Mantegna, P. Perego, M. Avogadro, and P. Cintas, Ultrason. Sonochem. **15**, 898 (2008).
6) T. S. H. Leong, T. J. Wooster, S. E. Kentish, and M. Ashokkumar, Ultrason. Sonochem. **16**, 721(2009).
7) M. Luque de Castro and F. Priego-Capote, Ultrason. Sonochem. **14**, 717 (2007).
8) Z. Xu and K. Yasuda, Jpn. J. Appl. Phys. **50**, 07HE07 (2011).
9) T. Yotsumoto, T. Morita, Y. Noiri, Y. Kojima, Y. Asakura, and S. Koda, Jpn. J. Appl. Phys. **53**, 07KE09 (2014).
10) K. Yasuda, T. T Nguyen, R. Okura, S. Nakayama, Y. Asakura, and J. Jin, Jpn. J. Appl. Phys. **54**, 07HE03 (2015).
11) M. Sivakumar, S. Y Tang, and K. W Tan, Ultrason. Sonochem. **21**, 2069 (2014).
12) C. D. Arvanitis, M. Bazan-Peregrino, B. Rifai, L. W. Seymour, and C.-C. Coussios, Ultrasound Med. Biol. **37**, 1838 (2011).
13) Y. Uemura, K. Sasaki, K. Minami, T. Sato, P. K. Choi, and S. Takeuchi, Jpn. J. Appl. Phys. **54**, 07HB05 (2015).
14) J. Yasuda, T. Miyashita, K. Taguchi, S. Yoshizawa, and S. I. Umemura, Jpn. J. Appl. Phys. **54**, 07HF21 (2015).
15) X. Qu, T. Azuma, R. Sugiyama, K. Kanazawa, M. Seki, A. Sasaki, and S. Takagi, Jpn. J. Appl. Phys. **55**, 07KF04 (2016).
16) E. A. Neppiras, IEEE Trans. Sonics Ultrason. **15**, 81 (1968).
17) T. Kikuchi and S. Sato, Jpn. J. Appl. Phys. **39**, 3158 (2000).
18) T. Uchida and T. Kikuchi, Jpn. J. Appl. Phys. **52**, 07HC01 (2013).
19) Y. Asakura, in *Sonochemistry and the Acoustic Bubbles,* ed. F. Grieser, P. Choi, N. Enomoto, H. Harada, K. Okitsu, and K. Yasui (Elsevier, Amsterdam, 2015) Chap. 5.

20) S. Nomura, S. Mukasa, M. Kuroiwa, Y. Okada, and K. Murakami, Jpn. J. Appl. Phys. **44**, 3161 (2005).
21) M. Shiiba, N. Okada, T. Uchida, T. Kikuchi, M. Kurosawa, and S. Takeuchi, Jpn. J. Appl. Phys. **53**, 07KE06 (2014).
22) M. Shiiba, N. Okada, M. Kurosawa, and S. Takeuchi, Jpn. J. Appl. Phys. **55**, 07KE16 (2016).
23) O. B. Wilson, in *Power Sonic and Ultrasonic Transducer Design*, ed. B. Hamonic and J. N Decarpigny (Springer-Verlag Berlin, Heidelberg, 1988) Chap. 1.
24) M. Hodnett, R. Chow, and B. Zeqiri, Ultrason. Sonochem. **11**, 441 (2004).
25) T. Uchida, H. Sato, S. Takeuchi, and T. Kikuchi, Jpn. J. Appl. Phys. **49**, 07HE03 (2010).
26) T. Uchida, S. Takeuchi, and T. Kikuchi, Jpn. J. Appl. Phys. **50**, 07HE01 (2011).
27) J. Frohly, S. Labouret, C. Bruneel, I. Looten-Baquet, and R. Torguet, J. Acoust. Soc. Am. **108**, 2012 (2000).
28) G. Iernetti, Acustica **24**, 191 (1971).
29) K. Yasui, T. Tuziuti, J. Lee, T. Kozuka, A. Towata, and Y. Iida, Ultrason. Sonochem. **17**, 460 (2010).
30) N. Okada, Y. Asakura, M. Shiiba, S. Takeuchi, T. Uchida, M. Yoshioka, T. Kikuchi, and M. Kurosawa, Proc. IEEE Int. Ultrason. Symp., 2013, p. 1121.
31) L. Thomas, C. Michael, S. Piotr, K. Kai, and J. Pablo, Ultrason. Sonochem. **27**, 22 (2015).
32) K. S. Suslick, Sci. Am. **260**, 80 (1989).
33) K. S. Suslick and T. J. Matula, *Encyclopedia of Electrical and Electronics Engineering* (Wiley, New York, 1999) p. 647.

Figure Captions

Fig. 1. Experimental setting for measurement of sound pressure and the broadband noise.

Fig. 2. Example of sound pressure spectrum at a driving frequency of 304 kHz and an electric power of 4 W.

Fig. 3. Sound pressure at the fundamental frequency and BIP as functions of the square root of the effective electric power applied to the transducer in low-electric-power range at driving frequencies of (a) 22 and (b) 488 kHz.

Fig. 4. (a) Experimental setting for the bubble observation and images obtained using ultrasonic diagnostic equipment in water (b) without and (c) with ultrasonic irradiation at a driving frequency of 488 kHz and an electric power of 1 W.

Fig. 5. Sound pressure at the fundamental frequency and BIP as functions of the square root of the effective electric power applied to the transducer when the effective electric power was changed from 0 to 100 W. The driving frequencies were (a) 22 and (b) 488 kHz.

Fig. 6. Sound pressures at the second harmonic and first ultraharmonic frequencies as functions of the square root of the effective electric power applied to the transducer at the driving frequencies of (a) 22, (b) 304, and (c) 488 kHz.

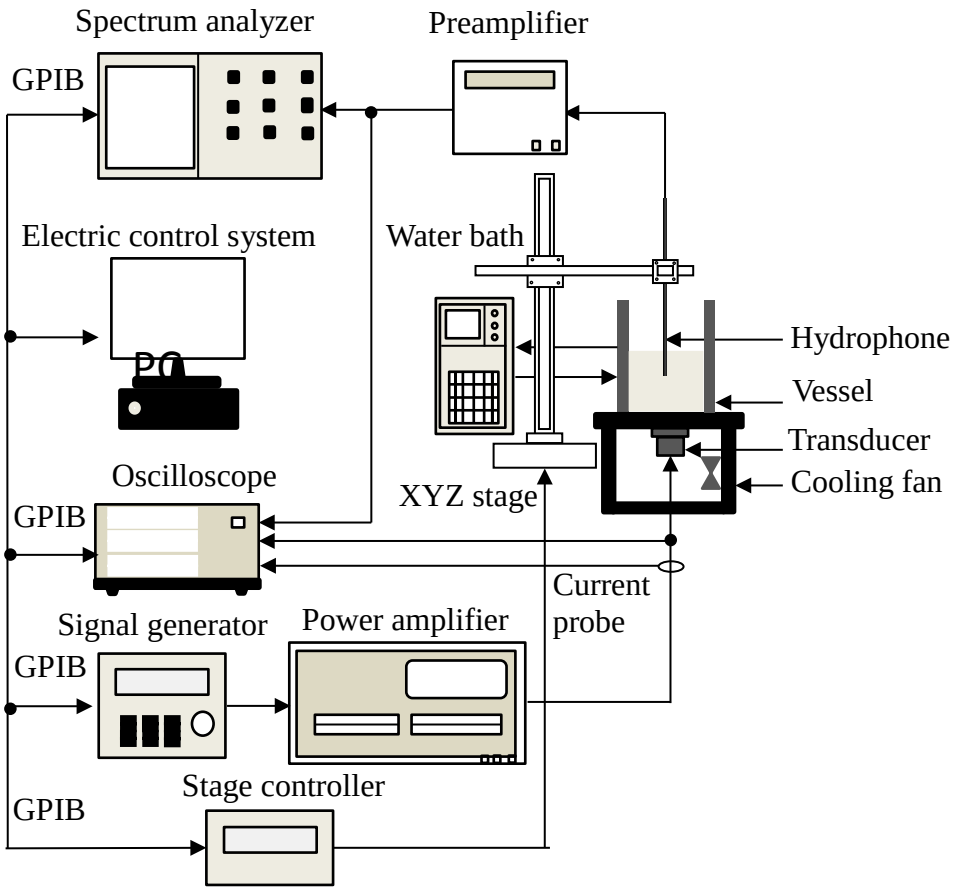
Spectrum analyzer
Preamplifier
GPIB
Electric control system
Water bath
PC
Hydrophone
Vessel
Transducer
Cooling fan
Oscilloscope
XYZ stage
GPIB
Current
probe
Signal generator
Power amplifier
GPIB
Stage controller
GPIB

Fig.1.

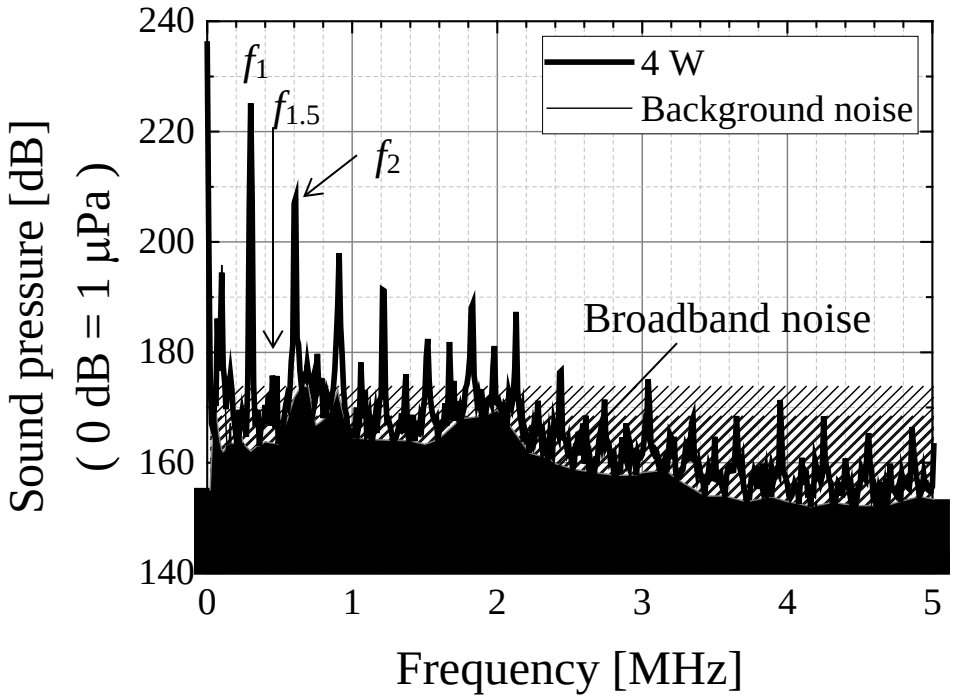
240
220
200
180
160
140
0
1
2
3
4
5
Sound pressure [dB]
(0 dB = 1 μPa)
Frequency [MHz]
f_1
$f_{1.5}$
f_2
4 W
Background noise
Broadband noise

Fig.2.

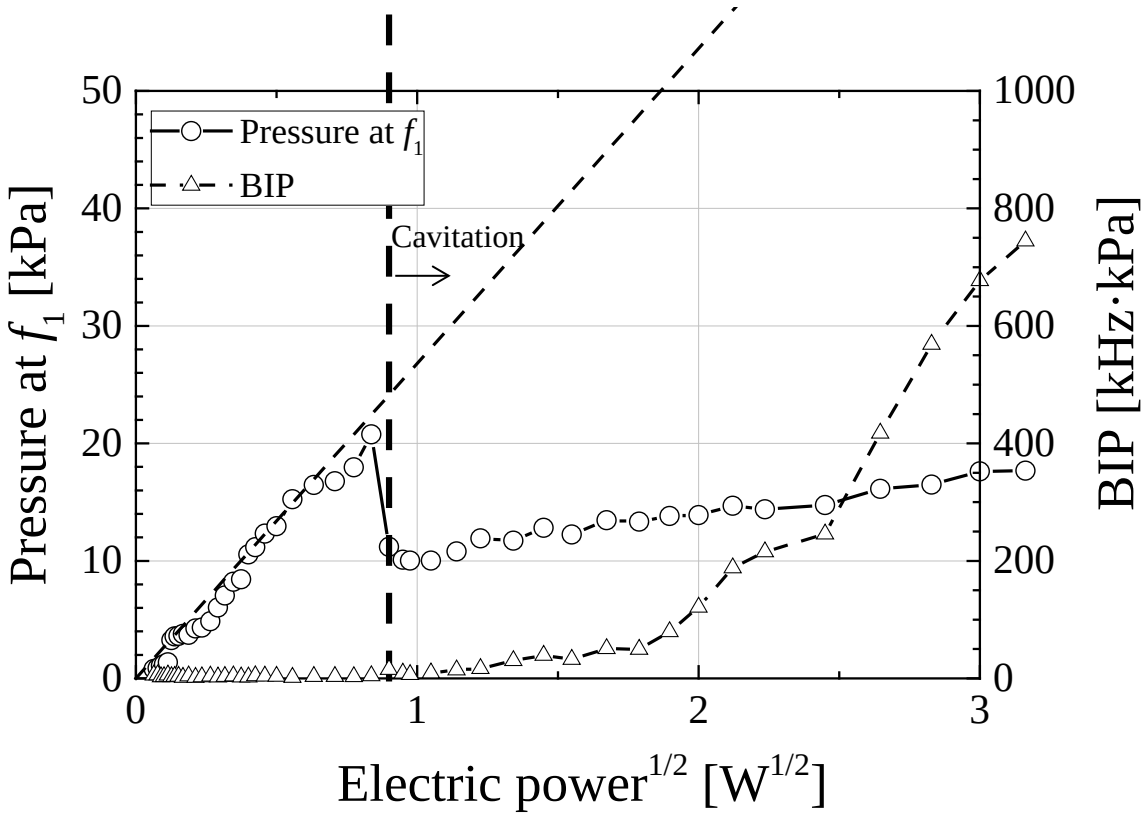
Pressure at f_1
BIP
Cavitation
Pressure at f_1 [kPa]
BIP [kHz·kPa]
Electric power$^{1/2}$ [W$^{1/2}$]
0
10
20
30
40
50
200
400
600
800
1000
1
2
3

Fig.3(a).

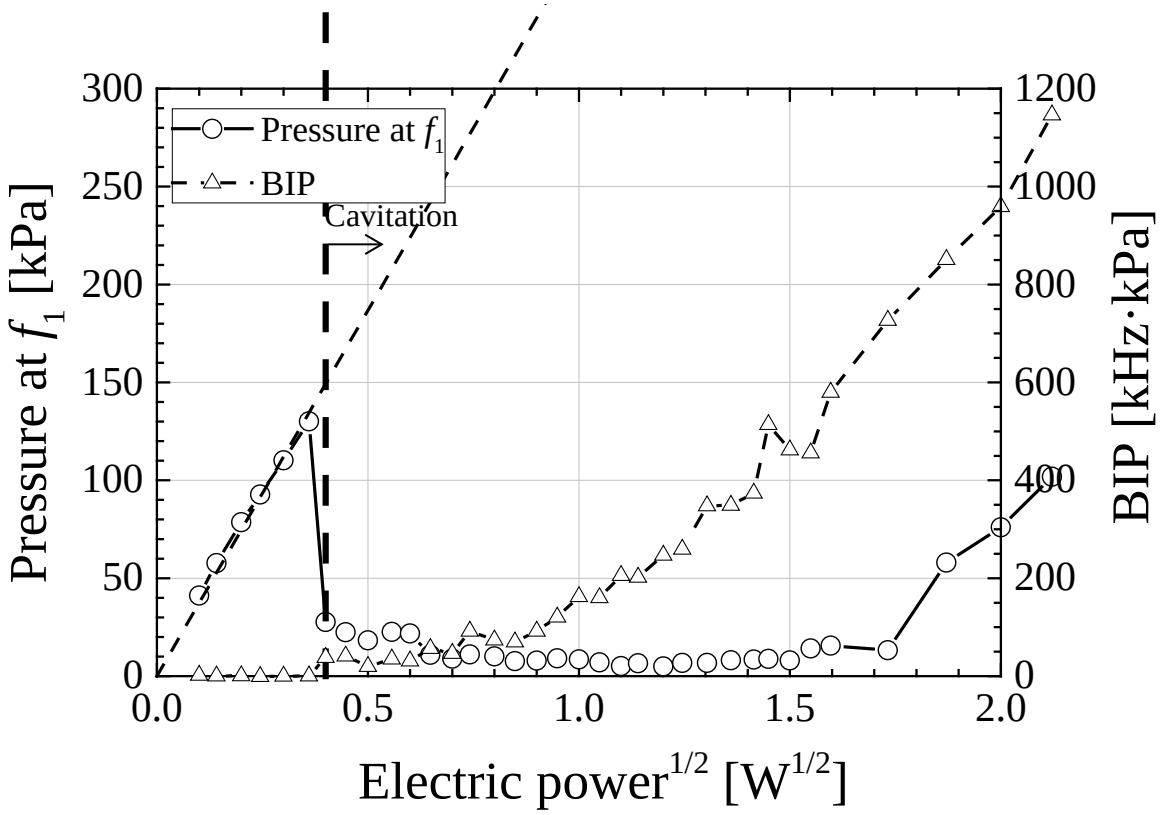
Pressure at f_1
BIP
Cavitation
Pressure at f_1 [kPa]
BIP [kHz·kPa]
Electric power$^{1/2}$ [W$^{1/2}$]
0
50
100
150
200
250
300
0
200
400
600
800
1000
1200
0.0
0.5
1.0
1.5
2.0

Fig.3(b).

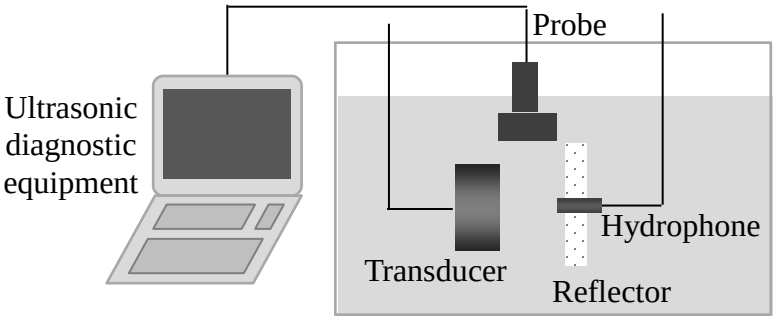
Probe
Ultrasonic
diagnostic
equipment
Hydrophone
Transducer
Reflector

(a)

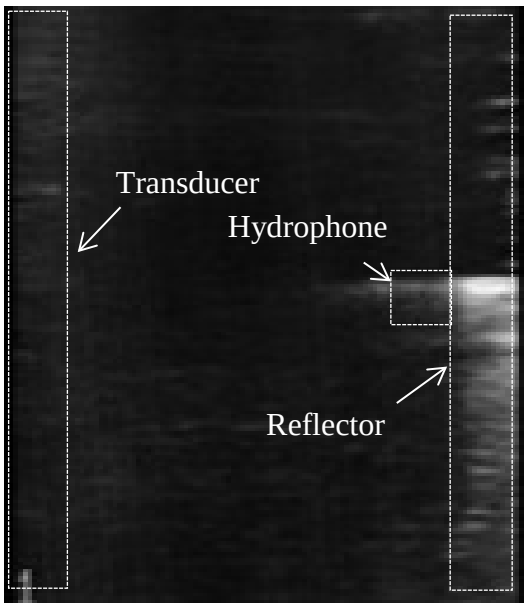
Transducer
Hydrophone
Reflector

(b)

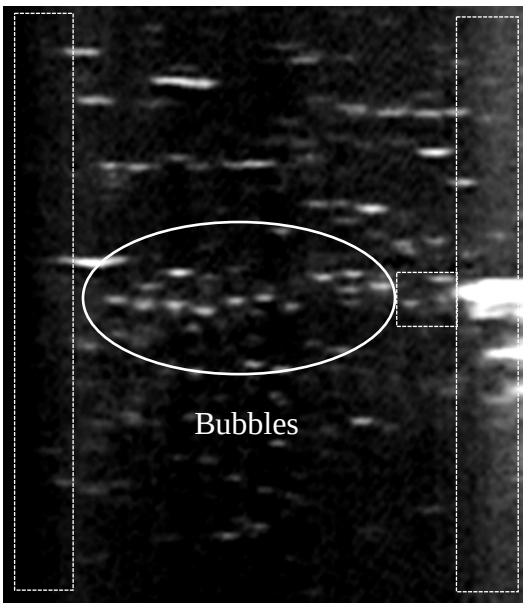
Bubbles

(c)

Fig.4.

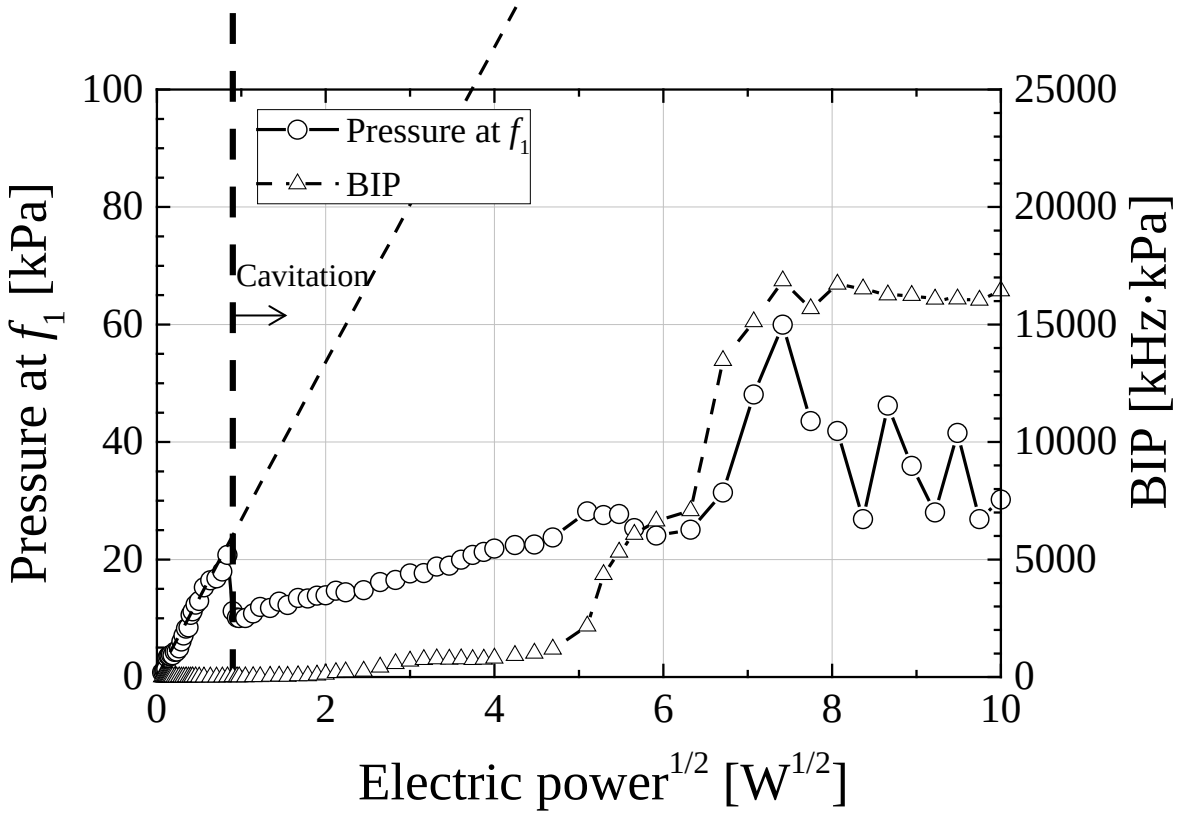
Pressure at f_1
BIP
Cavitation
Pressure at f_1 [kPa]
BIP [kHz·kPa]
Electric power$^{1/2}$ [W$^{1/2}$]
0
20
40
60
80
100
0
5000
10000
15000
20000
25000
0
2
4
6
8
10

Fig.5(a).

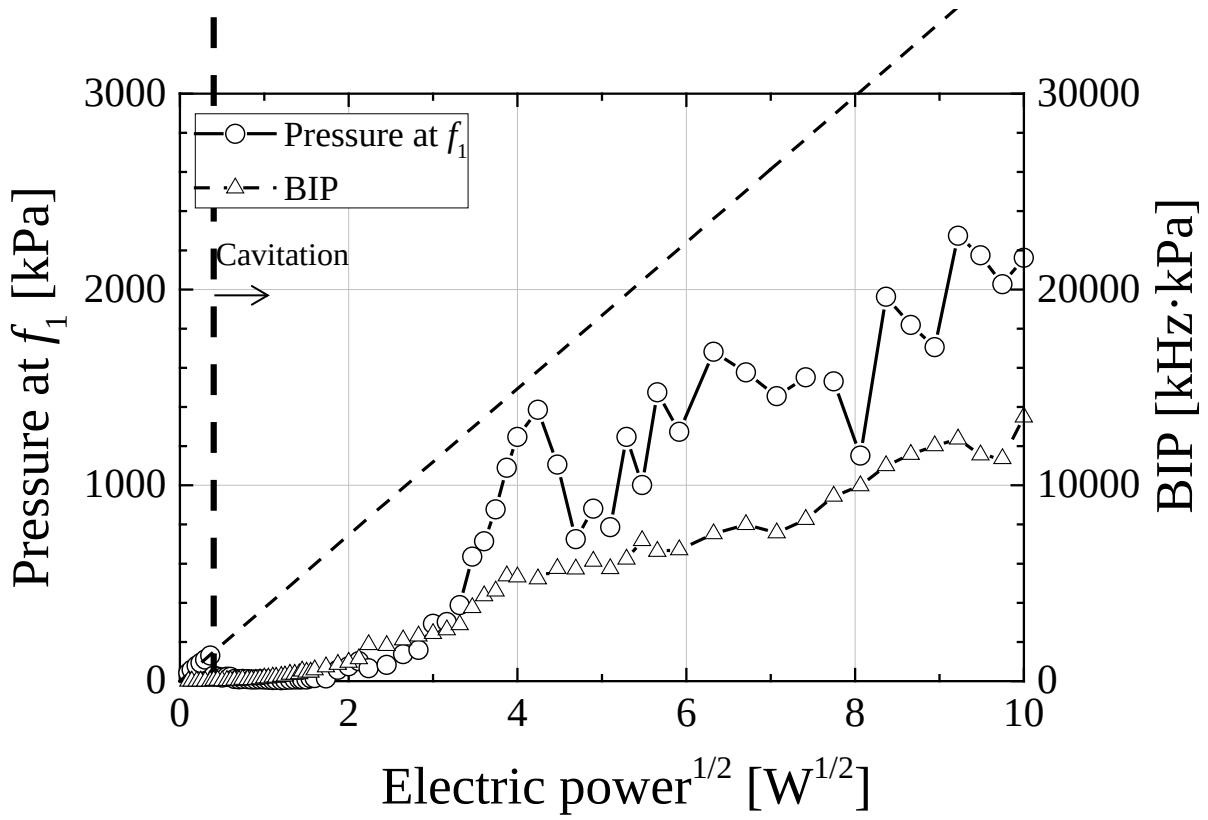
Pressure at f_1
BIP
Cavitation
Pressure at f_1 [kPa]
BIP [kHz·kPa]
Electric power$^{1/2}$ [W$^{1/2}$]
0
1000
2000
3000
10000
20000
30000
0
2
4
6
8
10

Fig. 5(b).

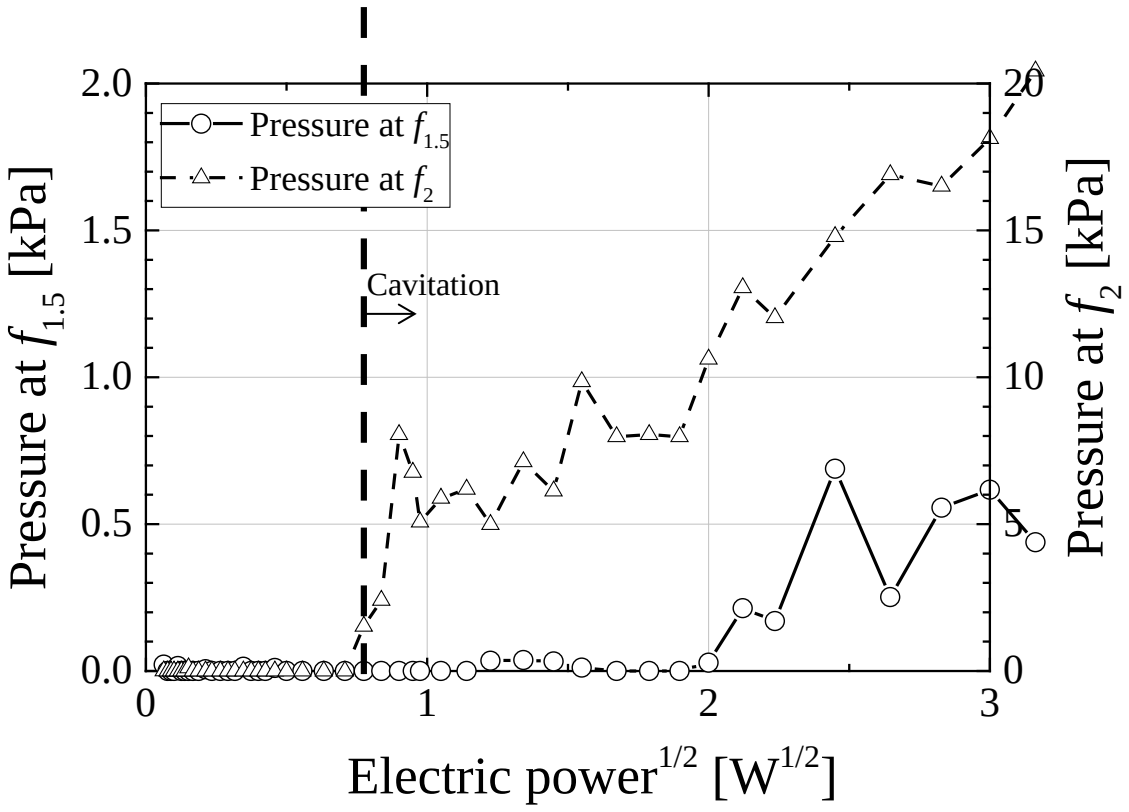
Pressure at $f_{1.5}$
Pressure at f_2
Cavitation
Pressure at $f_{1.5}$ [kPa]
Pressure at f_2 [kPa]
Electric power$^{1/2}$ [W$^{1/2}$]
2.0
1.5
1.0
0.5
0.0
20
15
10
5
0
0
1
2
3

Fig. 6(a).

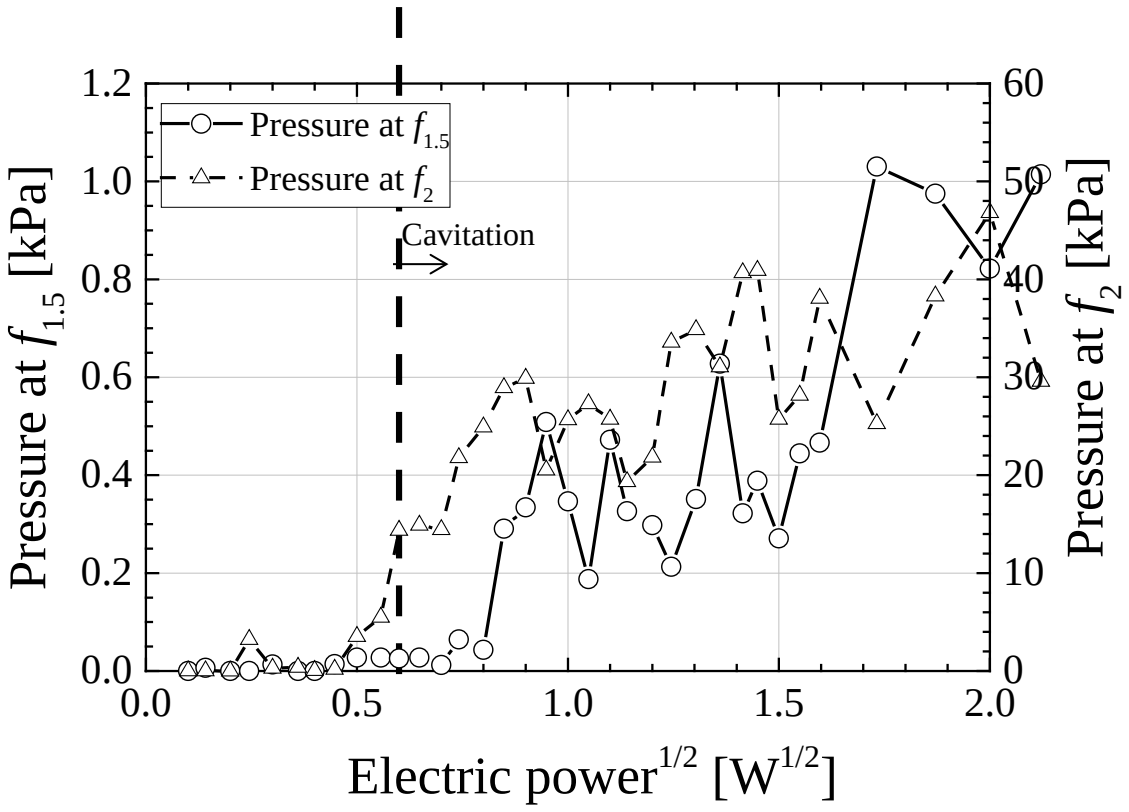
Pressure at $f_{1.5}$
Pressure at f_2
Cavitation
Pressure at $f_{1.5}$ [kPa]
Pressure at f_2 [kPa]
Electric power$^{1/2}$ [W$^{1/2}$]
0.0
0.2
0.4
0.6
0.8
1.0
1.2
0
10
20
30
40
50
60
0.0
0.5
1.0
1.5
2.0

Fig. 6(b).

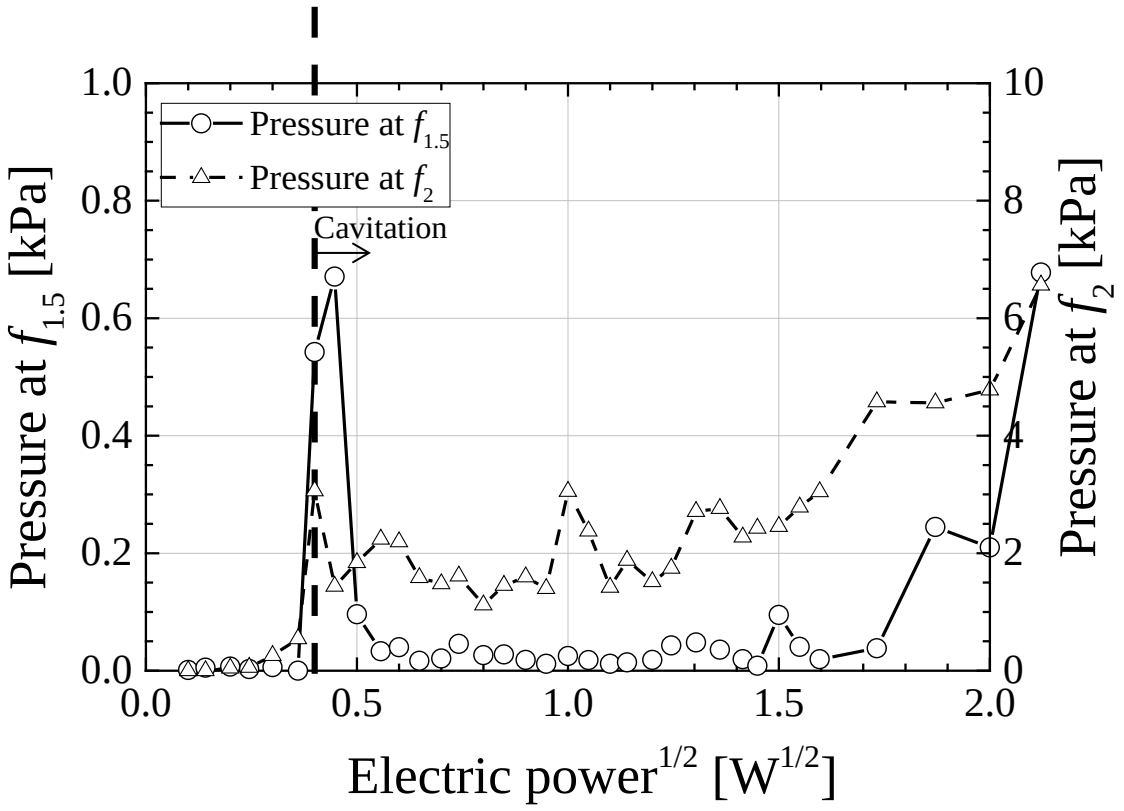
Pressure at $f_{1.5}$
Pressure at f_2
Cavitation
Pressure at $f_{1.5}$ [kPa]
Pressure at f_2 [kPa]
Electric power$^{1/2}$ [W$^{1/2}$]
0.0
0.2
0.4
0.6
0.8
1.0
0
2
4
6
8
10
0.0
0.5
1.0
1.5
2.0

Fig. 6(c).